ACS Photonics

pubs.acs.org/journal/apchd5

Article

Extended Quantum Tunnelling Distance in Planar Plasmonic Gaps

Ruizhao Yao, Danjun Liu,* Tao Yan, Sheng Lan, and Guang-Can Li*

Cite This: *ACS Photonics* 2026, 13, 1810−1817

Read Online

ACCESS | Metrics & More | Article Recommendations | Supporting Information

ABSTRACT: Light can drive charge transfer across metal nanogaps via quantum tunnelling processes, underpinning diverse molecular optoelectronic devices. However, such optical quantum tunnelling effects are usually significant at the subnanometer scale, which is not readily accessible. Here, we demonstrated that the threshold tunnelling gap distance, below which the quantum tunnelling effects become significant, strongly depends on the gap morphologies and can be significantly extended to >1.3 nm in planar plasmonic gaps. Furthermore, a phenomenological model was developed to illustrate how this threshold gap distance correlates with gap morphology. These findings provide new insights into quantum tunnelling effects in plasmonic nanogaps and point out how to relax the size requirement for accessing quantum tunnelling effects in plasmonic nanosystems, significant for quantum plasmonics and relevant applications.

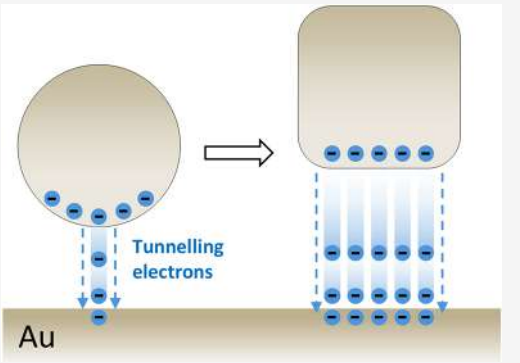

KEYWORDS: *quantum tunnelling, charge transfer, quantum plasmonics, plasmonic gaps, nanoparticle-on-mirror*

INTRODUCTION

Charge transfer between metal surfaces underpins diverse optoelectronic nanodevices and applications, such as single-molecule switches,[1,2] ultracompact light sources,[3,4] and scanning tunnelling microscopies (STM).[5,6] In the classical regime, these carrier transports can be triggered by external electric bias or intense optical field (like ultrashort laser pulses) induced surface photoemission,[7−12] with a tunnelling length up to the 10s nm scale. Through localized surface plasmon excitations,[13,14] quantum effects such as surface electron spill-out can also induce charge transfer across thin metal gaps.[15] However, such quantum tunnelling effects usually become significant at the subnanometer scale, not readily accessible through established fabrication approaches.[16,17] To harness such nonclassical effects for potential quantum applications, it is required to extend the observable quantum tunnelling regime to a larger size scale,[18] but it remains unknown to what extent this boundary can be pushed.

Light-driven quantum tunnelling effects in plasmonic gaps were mainly probed through associated plasmonic responses and intensively addressed in individual nanoparticle dimer structures, the simplest plasmon coupling system.[15,16,19−23] In such nanoparticle pairs, the dominant plasmonic response originates from bonding dipolar plasmon (BDP) coupling between the two particle plasmons and is significantly modified by quantum tunnelling effects. Early studies based on the full quantum mechanical model revealed a nonmonotonic spectral shifting of the BDP resonance with decreasing dimer gap distances. This defines a threshold gap distance (termed d_0 hereafter) at which quantum tunnelling effects come into play, typically ∼0.4 nm for small nanosphere dimer systems (diameter <10 nm).[24,25] Although full quantum analysis is technologically limited to small plasmonic structures, it predicted extended threshold gap distances for larger plasmon coupling systems.[24] A line of studies examined the practical plasmonic dimers gaps formed with particle size >30 nm, resolving a d_0 typically in the range of ∼0.5−0.8 nm.[16,22,26,27] Particularly, a recent study tracked particle size-dependent d_0 for individual dimer gaps, finding that it increases with particle diameter.[18] Following analysis based on the quantum-corrected model (QCM) attributed the extended d_0 of larger nanospheres to increased surface curvature,[18] which results in higher effective gap conductance compared to small plasmonic particle pairs.[28]

In the extreme case, spherical particle dimers with infinitely large particle sizes give rise to planar gap surfaces. The infinite surface curvature of such planar gap junctions suggests a significantly extended threshold tunnelling gap distances with respect to curved gap surfaces. Similar planar gap configurations can be formed with individual nanocube dimers,[29,30] which have been found to exhibit an enhanced quantum tunnelling rate and even produce charge transfer plasmon (CTP),[31] a phenomenon conventionally associated with highly conductive nanogap.[32] Verifying the extended d_0 of these nanocube dimer gaps seems practicable, but it requires

Received: October 27, 2025
Revised: March 11, 2026
Accepted: March 13, 2026
Published: March 18, 2026

https://doi.org/10.1021/acsphotonics.5c02595
ACS Photonics 2026, 13, 1810−1817

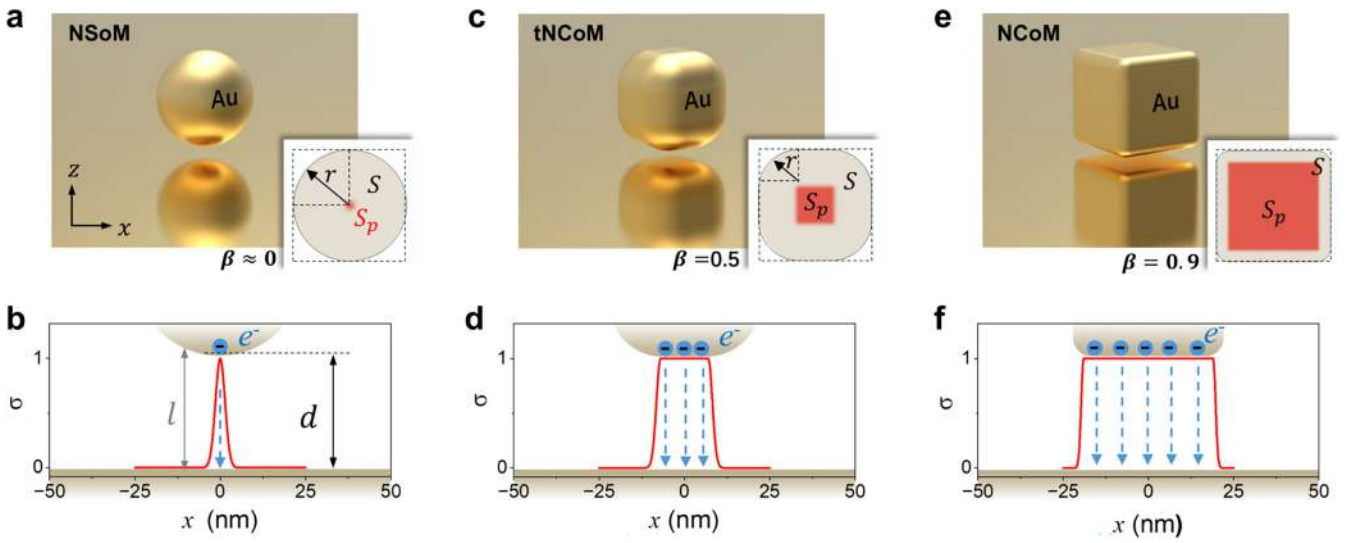

Figure 1. Schematic illustration of the quantum tunnelling channel in plasmonic gaps with controlled geometry morphologies. (a, c, e) The geometry transition from a nanosphere-on-mirror (NSoM) construct (a), then a moderately truncated nanocube-on-mirror (tNCoM) configuration (c), to a NCoM with small corner curvatures (e). A geometry parameter (β) defined by the size ratio between the planar gap area (S_p, the red domain) and the nanoparticle cross section (S, the white area), is used to characterize the morphology of plasmonic gaps formed in these nanoparticle-on-mirror (NPoM) nanoconstructs. (b, d, f) Normalized conductivity (σ) profiles at the gap center ($z = d/2$) calculated based on the quantum-corrected model (QCM), indicating the maximum width of the quantum tunnelling channel that electrons can transfer through. In calculations, all the lateral sizes (diameter or side length) of the nanoparticles are 50 nm and all the gap sizes (d) are 1 nm. The curvature (r) of the round corners of the tNCoM and NCoM constructs are 18 and 6 nm, respectively.

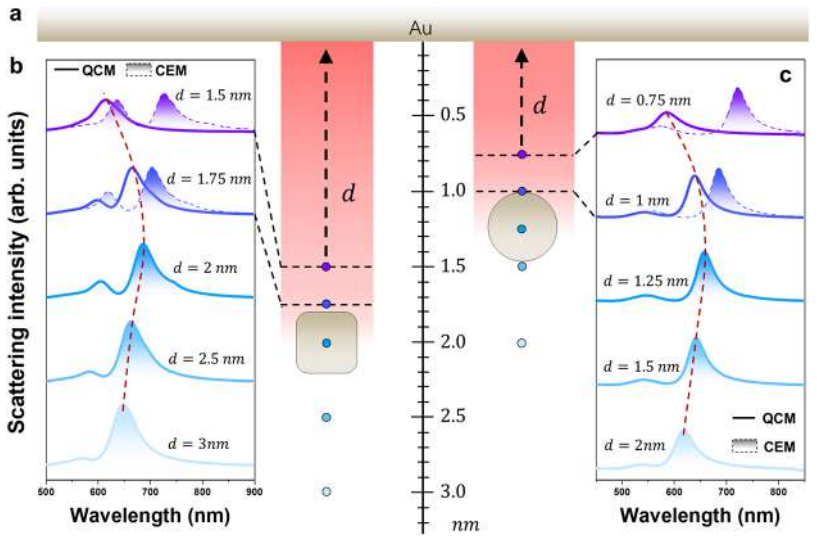

Figure 2. Quantum tunnelling effect modified scattering plasmon responses of individual NCoM and NSoM constructs. (a) Schematic of individual gold nanocubes (left) and nanospheres (right) respectively approaching a gold mirror. (b, c) Gap distance-dependent scattering spectra of individual NCoM (b) and NSoM (c) constructs, calculated based on both the classical electromagnetism model (CEM) and quantum-corrected model (QCM). Dashed lines (red) indicate the spectral shifting of the dominant coupling plasmon resonances.

nanometer-scale control of the gap distances and high-precision alignment of the nanocube facets, which are technically demanding.[33−35]

In this paper, instead of using nanocube dimer structures, we employed planar gaps formed in the gold nanocube-on-mirror (NCoM) construct to resolve the maximum tunnelling gap distance, the threshold below which quantum tunnelling effects become significant. Such NCoMs exhibit similar plasmonic responses to individual nanocube dimers, yet they constitute a preferred plasmon coupling configuration that benefits from their ease of fabrication.[36−38] Supported by quantum-corrected electromagnetic simulations and scattering spectroscopy, we tracked the gap distance-dependent plasmon resonances of individual NCoMs and revealed a significantly extended tunnelling gap distance up to >1.3 nm. This largely relaxes the size requirement for accessing quantum effects in plasmonic gaps, conventionally limited to the subnanometer scale.

RESULTS AND DISCUSSION

To illustrate how the gap morphology affects quantum tunnelling (QT) effects in individual plasmonic gaps, we began by inspecting nanoparticle-on-mirror (NPoM) constructs with controlled gap morphologies (see the insets of

https://doi.org/10.1021/acsphotonics.5c02595
ACS Photonics 2026, 13, 1810−1817

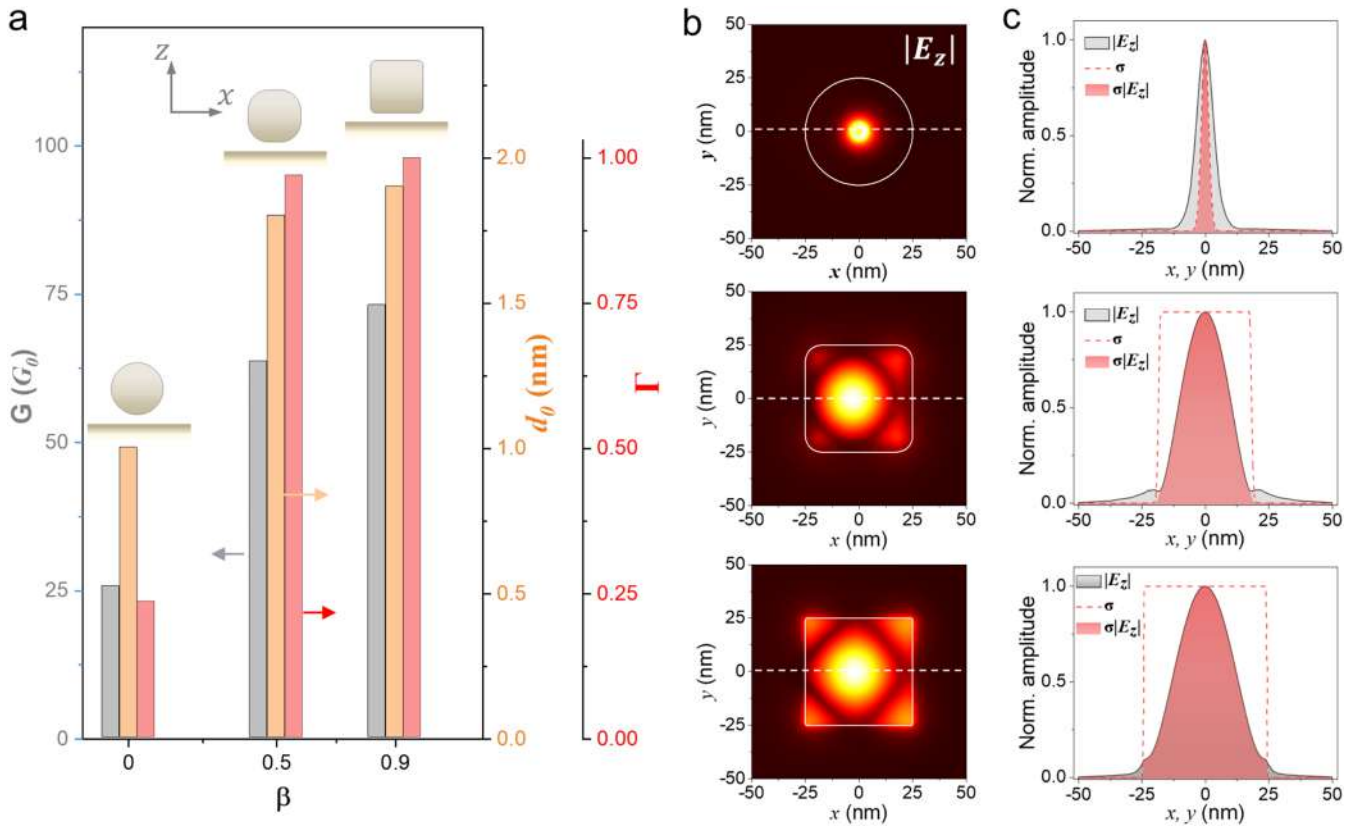

Figure 3. Correlation of the threshold tunnelling gap distance with gap morphology. (a) Morphology (β)-dependent threshold tunnelling gap distance (d_0, orange), gap conductance (G, gray) and filling factor (Γ, red), calculated for the structures as indicated. (b) The lateral distribution of normalized $|E_z|$ at the gap center ($z = d/2$) of structures shown in (a). (c) Comparison between the line-cut of $|E_z|$ (extracted from (b)), conductivity profile (extracted from Figure 1), and the product between them, i.e., $\sigma|E_z|$, all normalized to their maximum value. The geometry parameters in these calculations are the same as those shown in Figure 1, except for the gap distances controlled in (a).

Figure 1a, c, and e). In this NPoM architecture, continuously reducing the curvatures (r) of the round corners of single nanocubes results in the structural evolution from a nanosphere-on-mirror (NSoM) configuration to a typical nanocube-on-mirror (NCoM) construct. As depicted in Figure 1a, c and e, the size ratio (β) between the area of the planar gap facet (S_p) and the whole nanoparticle cross section (S), i.e., $\beta = S_{p/S}$, is used to characterize the morphology of different nanoparticle-mirror gaps. Optically exciting these nanoparticle-on-mirror (NPoM) structures can induce near-field coupling between the particle plasmons and their images in the mirror,[37] producing strong light confinement in the gap region and enabling quantum tunnelling events when the gap distance is sufficiently small.

Quantum tunnelling across the plasmonic gaps results in conductive coupling between the facing gap interfaces. This conductive coupling modifies the gap-associated plasmon responses, which can be described using the so-called quantum-corrected model (QCM).[39−41] The QCM theory views the gap region as bridged by a fictitious conductive material, with the conductivity determined by the separation distances of facing gap surfaces (l, see Figure 1b) as well as the frequency (ω) of light driving the quantum tunnelling process (for more details, see Supporting Information). Based on this treatment, we calculated the conductivity profiles of the different NPoM nanogaps. As displayed in Figure 1b, d, and f, the plasmonic gaps with different morphologies exhibit dramatically different conductivity profiles. For plasmonic gaps with the same gap distance d (the minimal separation distance between the facing gap interfaces), the one with a larger morphology parameter β exhibits a broader conductivity line width, thereby providing a wider quantum tunnelling channel for more surface charges to transfer through. This also suggests that the onset of quantum tunnelling effects could be spotted at a larger gap distance in planar gaps than in curved ones.

Significant quantum tunnelling effect in gapped metal structures reduces surface charges and weakens gap-mediated plasmon coupling interactions. This modifies the structural plasmon responses, allowing quantum tunnelling events to be probed. To confirm and resolve the extended threshold tunnelling gap distance d_0 for planar plasmonic gaps, we simulated the scattering plasmon responses of individual NCoM structures with decreasing gap distances and compared them with the NSoM construct (depicted in Figure 2a). As shown in Figure 2b,c, when the gap distances are relatively large ($d \geq 2$ nm), the scattering responses of both the NCoM and NSoM constructs are dominated by a strong antenna plasmon resonance. This radiative antenna mode originates from the vertical bonding between the particle dipolar plasmon and its image induced in the mirror, and red-shifts when the gap distances are further reduced (see the Mode analysis in Supporting Information). For the NSoM gaps, several previous studies resolved a blue-shifting of the antenna resonance when the gaps are further reduced to below 1 nm, in line with our observation shown in Figure 2c. Such blue-shifting resonances

https://doi.org/10.1021/acsphotonics.5c02595
ACS Photonics 2026, 13, 1810−1817

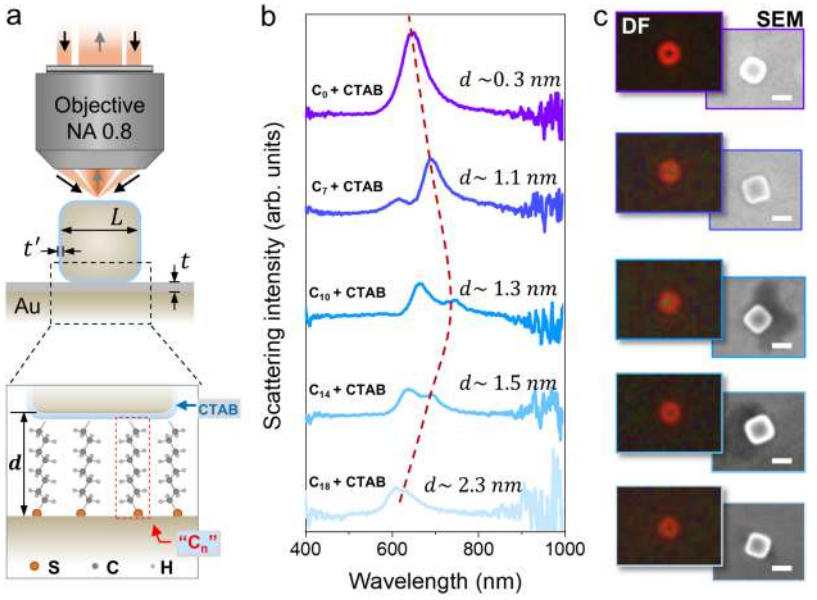

Figure 4. Measurement of the scattering plasmon responses of individual NCoM structures with controlled gap distances. (a) Schematic illustration of the dark-field microscope setup (upper) and the content of NCoM gaps. The gap distance (d) of individual NCoM structures is determined by the thickness of the CTAB layer coated on nanocubes (t') and a monolayer of alkanethiol molecules self-assembled on a gold film (t), i.e., $d = t + t'$. Cn specifies individual alkanethiol molecules containing n carbon atoms. (b) The typical scattering spectra of individual NCoMs with different gap distances. (c) Corrective dark-field (DF) images (left) and scanning electron micrographs (SEM, right) of the NCoM structures in (b). The scale bar in each SEM image is 50 nm.

can be attributed to the intensifying quantum tunnelling across the subnanometer gap, which is also evidenced by the significant deviation of the QCM simulation results from the classical electromagnetism model (CEM). The nonmonotonic resonance shifting as well as the divergence between the QCM and CEM simulations resolves a threshold gap distance $d_0 \approx 1$ nm, which marks the onset of quantum tunnelling effects. It should be noted that this threshold value is slightly larger than the d_0 reported for individual spherical nanodimer gaps (typically ~0.5−0.8 nm).[16,18,22] We attributed this to the asymmetric gap geometry of individual NSoM constructs, in which the underlying planar mirror can be seen as a plasmonic particle with infinite large diameter (or curvature),[42] thus increasing the gap conductivity and widening the quantum tunnelling channel.

Similar plasmon evolution characters have been observed for the NCoM constructs with varying gap distances (see Figure 2b). However, their scattering responses calculated with the QCM approach start to deviate from the CEM simulations at a significantly larger gap distance ($d_0 \approx 1.75$ nm) with respect to the NSoM geometry. Such a large tunnelling distance has never been resolved in plasmonic nanostructures with curved gap surfaces, but it is possible for planar nanogaps. To illustrate how gap morphology affects the threshold tunnelling distance d_0, we extracted the d_0 of NPoM constructs with different morphology parameters (β). As shown in Figure 3a, the threshold tunnelling distance d_0 increases monotonically with increasing β, basically following the evolution of β-dependent gap conductance. Nevertheless, the d_0 vs. β seems to evolve to an upper limit capped by the NCoM construct, yet alongside an ever-increasing gap conductance. This trend consists with previous theoretical studies involving planar dimer gaps,[41] and is further confirmed by experimental observations for the NCoM constructs (as will be seen later), suggesting that the extended d_0 for larger β cannot be attributed solely to increased gap conductance.

The quantum tunnelling process across the NPoM gaps is driven by the plasmonic fields localized in the center region (see Figure 3b). This hot spot domain is regulated by the lateral distribution of gap conductivity, creating the effective quantum tunnelling channel across a gap. For the NSoM configuration, the gap conductivity profile is found to be much narrower than the associated plasmonic field profile (upper panel in Figure 3c), suggesting that only a small fraction of the plasmon-induced surface charges can tunnel across the gap. This marginally modifies the structural plasmon responses and explains why quantum tunnelling effects are only observable in subnanometer-sized plasmonic gaps. In contrast, the lateral distribution of the NCoM gap conductance is much broader than the associated plasmonic field profile (see middle and bottom panels in Figure 3c), making it possible to deplete all the surface charges via a quantum tunnelling process. Based on this phenomenological treatment, we define a filling factor Γ to evaluate the effect of quantum tunnelling process on the structural plasmon responses; it writes as

$$\Gamma = \frac{\int_S \hat{\sigma}|E_z|\mathrm{d}s}{\int_S |E_z|\mathrm{d}s} \tag{1}$$

where S denotes the planar integration domain across the gap center (z -cut plane), $\hat{\sigma}$ is the normalized gap conductivity and E_z the dominant plasmonic field component inside the gap. The product $\hat{\sigma}|E_z|$ determines the tunnelling domain and measures the width of the effective quantum tunnelling channel across a gap. The Γ of NPoM constructs with different morphology parameters (β) are calculated and displayed in Figure 3a. The Γ first rapidly increases with increasing β, then slowly evolves and finally saturates at large β, following precisely the evolution trend of d_0 vs. β. In particular,

https://doi.org/10.1021/acsphotonics.5c02595
ACS Photonics 2026, 13, 1810−1817

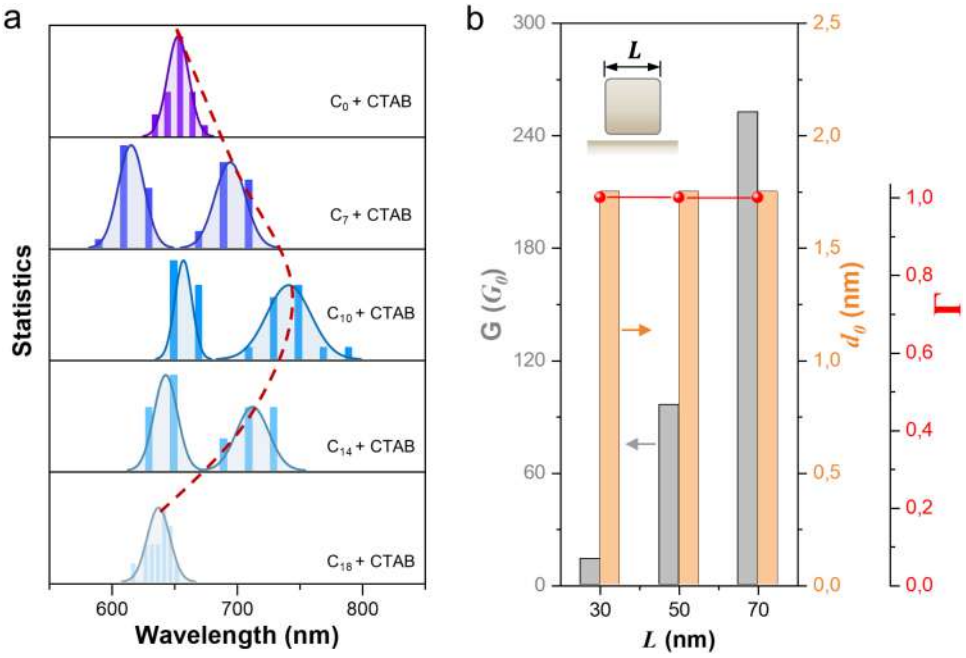

Figure 5. (a) Statistics of spectral wavelengths of the dominant NCoM resonances. The measurement for each gap distance was performed over hundreds of individual NCoM entities. (b) Particle-size dependent threshold tunnelling gap distance (d_0, orange bar), gap conductance (G, gray bar) and filling factor (Γ, red line) for NCoM constructs. The round corner curvatures of the nanocubes are set as 5 nm in the simulations.

the NSoM ($\beta \approx 0$) configuration exhibits a much smaller filling factor (Γ~0.23) than the NCoM gaps with $\beta \geq 0.5$ (showing Γ > 0.9), suggesting the NSoM plasmon resonances are much less affected by the tunnelling events than the NCoM constructs. This also explains why the threshold gap distance for quantum tunnelling effects in NCoM constructs is significantly larger than the NSoM configuration.

To experimentally verify the extended threshold tunnelling gap distance in planar plasmonic gaps, we fabricated gold NCoM structures with controllable gap distances (as depicted in Figure 4a). Individual nanocubes are spaced from the underlying gold mirror by a self-assembled monolayer (SAM) of alkanethiol molecules, plus a CTAB (Cetyltrimethylammonium Bromide) bilayer coated on the nanoparticle (as surfactant, with reduced thickness ~0.25 nm, see Supporting Information).[43−45] Controllable gap distances are achieved by employing alkanethiol linkers with varying chain lengths, which depend on the number (n) of constituent carbon atoms. Here we chose the molecular linkers with n = 0, 7, 10, 14 and 18, which together with the CTAB coating layer, give rise to a set of gap distances of ~0.3, 1.1, 1.3, 1.5, and 2.3 nm, respectively (for more details, see Supporting Information).

Figure 4b shows the typical scattering spectra of individual NCoMs (cube size L = 50 ± 5 nm) with different spacer thicknesses, captured using a dark-field objective with high collection efficiency (NA = 0.8). These scattering spectra well reproduce the spectral characters displayed in Figure 2b, with the main plasmon resonances initially red-shifting with decreasing gap distances and then blue-shifting when the gap is narrowed to below a critical distance at approximately 1.3 nm (corresponding to the layer thickness of C_{10} + CTAB). This threshold gap distance is slightly smaller than the simulated threshold tunnelling distance resolved for the NCoM gaps shown in Figure 2b. However, the molecular gap content in the experimental condition is expected to lower the tunnelling barrier,[18,46−48] and give rise to a larger threshold gap distance compared to air gaps. This discrepancy could be attributed to underestimation of the molecular gap distances, to which the minimum evaluation value is assigned for each kind of molecular gap (as detailed in the Supporting Information). It should be noted that the split resonances observed for gaps of C_7, C_{10} and C_{14} (Figure 4b) arise from the plasmon hybridization between the antenna plasmon mode and the waveguide-like cavity mode emergent at small gap distances.[36,37] Nevertheless, the waveguide-like plasmon mode is essentially subradiative, a so-called dark mode. It gains radiation strength through mode hybridization with the antenna mode, so the total scattering responses of individual NCoMs are featured by the radiative antenna mode character, as evidenced by the doughnut-shaped scattering pattern observed in the dark-field (DF) images of individual NCoMs (Figure 4c).[49,50] Intensifying quantum tunnelling reduces also the charge densities associated with these subradiative waveguide modes, not only blue-shifting their resonance wavelengths but also weakening their strengths. As seen in Figure 4b, the waveguide resonances completely vanished for d < 1 nm, leaving the antenna mode resonance dominant.

Similar measurements as in Figure 4 were repeatedly performed over hundreds of NCoMs with varying gap distances, from which a statistic of the resonance wavelengths was extracted and shown in Figure 5a. Due to the inhomogeneity in nanocube sizes (see Supporting Information), the NCoM resonances for each gap distance exhibit significant fluctuations in their spectral positions. Despite this, tracking the average spectral positions of these dominant plasmon resonances still resolves a nonmonotonically shifting trend with decreasing spacer thickness. A crossover can be clearly identified for the C_{10}-associated gap distance, which corresponds to a threshold tunnelling gap distance of ~1.3 nm (plus the CTAB coating), in line with the QCM simulations shown in Figure 2b. Such excellent agreement is astounding, given the large spectral fluctuations of the resonance

https://doi.org/10.1021/acsphotonics.5c02595
ACS Photonics 2026, 13, 1810−1817

wavelengths; it appears that the threshold gap distance of QT effects is invariant to the nanocube sizes. To further confirm this, we simulated the particle size-dependence of the threshold tunnelling gap distance for individual NCoM structures. As shown in Figure 5b, the threshold gap distance d_0 for each particle size indeed remains constant (~1.75 nm) with extending surfaces (L). To shed more light on this, we evaluated the filling factors (Γ) of these NCoM constructs according to eq 1. It turns out that all the Γ are nearly identical and approximate to the maximum value, i.e., $\Gamma \sim 1$. Further extending the lateral gap width continuously increases the conductance of NCoM gaps but does not lift the influence of QT effects on the plasmon responses. Together with the d_0 vs. L shown in Figure 5b, it can be concluded that an ultimate limit of the threshold tunnelling gap distance exists for these plasmonic nanogaps. Such extreme plasmonic gaps feature a planar metal−insulator−metal (MIM) configuration, as formed in the NCoM constructs, nanocube dimers and between nanoparticles having relatively large facets.[51,52]

It should be noted that, in the above discussions, verifying the extended threshold tunnelling gap distance of plasmonic junctions is performed by tracking the plasmonic responses. The exact value of this threshold depends on the sensitivity of the plasmon resonance to quantum tunnelling events. Beyond this threshold gap distance, the quantum tunnelling process is too weak to be probed via plasmon responses. Besides, we would like to emphasis again that the electron tunneling discussed in this study is limited to the quantum effect driven process, which is much different from other classical and nonlinear tunnelling effects, for example, conductive bridging guided charge transfer,[53,54] intense electric or optical field-induced surface photoemission. Particularly, the photoemission process ejects electrons into the gap, which can tunnel through a gap spanning up to 10s nanometers, depending on the electric or optical bias amplitude applied.[7−12] In contrast, the quantum tunnelling originates from the quantum mechanical effect, like the surface electron spilling-out, is not so sensitive to the strength of external excitations.[21] This quantum tunnelling is significant at the atomic length scale and usually observable in between nearly touching metal surfaces.[55] In this regard, extending this quantum tunnelling regime to a larger length scale has significant implications for quantum nano-optics and relevant applications. Following the QCM treatment (as described in the Supporting Information), this quantum tunneling distance may be further extended by trying other kinds of molecular gap content, but detailed discussion on this topic is beyond the scope of this study.

CONCLUSIONS

In summary, we've examined the quantum tunnelling effects in plasmonic gaps with different morphologies, and revealed a significantly extended threshold tunnelling gap distance (d_0) below which quantum tunnelling effects become significant. A phenomenological model was developed to illustrate how this threshold gap distance is correlated with the gap morphology, successfully explaining why a subnanometer threshold tunnelling gap distance was found for curved plasmonic gaps and why planar nanogaps exhibit the maximum d_0 among various geometry configurations. Both numerical simulation and experimental measurement over the nanocube-on-mirror constructs validated the model and revealed the ultimate limit of the threshold tunnelling gap distance, which is greater than 1.3 nm. Such a significant extension of the threshold tunnelling gap distances relaxes the size requirement for accessing quantum tunnelling effects in plasmonic nanostructures, thereby facilitating the fabrication of quantum plasmonic systems, relevant to quantum nanophotonics and associated applications.[56,57]

METHODS

Sample Preparation

CTAB (Cetyltrimethylammonium Bromide) capped gold nanocube colloids were purchased from Nanoseedz, Inc. The side length of individual nanocubes is ~50 nm, and the CTAB coating is ~1 nm in thickness. These colloidal nanoparticles are then sparsely dispersed on a template-stripped gold film that possesses an atomic-scale surface smoothness. Before the particle deposition, alkanethiol molecules with different chain lengths are self-assembled on the film following the protocol in ref 58.

Single-Nanoparticle Scattering Spectroscopy

The scattering plasmon resonances of individual nanocubes are characterized using a reflective-type dark-field microscope (BX 51, Olympus) equipped with a spectrometer. A dark-field objective with NA = 0.8 was used to focus a hollow white light beam on the sample and simultaneously collect the scattered light from individual nanoparticles. The scattered light was then delivered through a tube lens to a CCD camera (Retiga R6, Teledyne Photometrics) for imaging or the spectrometer (QE Pro, Ocean Optics) for spectral analysis.

Numerical Simulations

A commercial finite element solver (COMSOL Multiphysics) was used to simulate the electromagnetic response of individual nanoparticle-on-mirror structures. A quantum-corrected model incorporating the quantum tunnelling effects in plasmonic nanogaps was embedded into the classical electromagnetic framework to simulate quantum-modified plasmonic responses of differently shaped NPoM nanostructures (for more details, see Supporting Information).

ASSOCIATED CONTENT

Supporting Information

The Supporting Information is available free of charge at https://pubs.acs.org/doi/10.1021/acsphotonics.5c02595.

Details on the sample characterization, implementation of the quantum-corrected model, and the approach to evaluate the gap distances of nanocube-on-mirror constructs with different molecular linkers (PDF)

AUTHOR INFORMATION

Corresponding Authors

Danjun Liu − *Guangdong Provincial Key Laboratory of Nanophotonic Functional Materials and Devices, Guangdong Basic Research Centre of Excellence for Structure and Fundamental Interactions of Matter, School of Optoelectronic Science and Engineering, South China Normal University, Guangzhou 510006, China*; Email: danjun.liu@scnu.edu.cn

Guang-Can Li − *Guangdong Provincial Key Laboratory of Nanophotonic Functional Materials and Devices, Guangdong Basic Research Centre of Excellence for Structure and Fundamental Interactions of Matter, School of Optoelectronic Science and Engineering, South China Normal University, Guangzhou 510006, China*; orcid.org/0000-0002-9903-8900; Email: Guangcan.li@m.scnu.edu.cn

https://doi.org/10.1021/acsphotonics.5c02595
ACS Photonics 2026, 13, 1810−1817

Authors

Ruizhao Yao − *Guangdong Provincial Key Laboratory of Nanophotonic Functional Materials and Devices, Guangdong Basic Research Centre of Excellence for Structure and Fundamental Interactions of Matter, School of Optoelectronic Science and Engineering, South China Normal University, Guangzhou 510006, China;* orcid.org/0009-0008-2967-550X

Tao Yan − *Guangdong Provincial Key Laboratory of Nanophotonic Functional Materials and Devices, Guangdong Basic Research Centre of Excellence for Structure and Fundamental Interactions of Matter, School of Optoelectronic Science and Engineering, South China Normal University, Guangzhou 510006, China*

Sheng Lan − *Guangdong Provincial Key Laboratory of Nanophotonic Functional Materials and Devices, Guangdong Basic Research Centre of Excellence for Structure and Fundamental Interactions of Matter, School of Optoelectronic Science and Engineering, South China Normal University, Guangzhou 510006, China;* orcid.org/0000-0002-7277-0042

Complete contact information is available at: https://pubs.acs.org/10.1021/acsphotonics.5c02595

Author Contributions

G.C.L. and D.J.L. designed and supervised the project. R.Y. fabricated the samples, set up the experimental rigs, performed experimental measurements, and conducted electromagnetic numerical simulations. T.Y. and S.L. assisted in sample characterization and relevant optical spectroscopy. G.C.L. wrote and finalized the manuscript with input from all the authors.

Funding

The National Natural Science Foundation of China (Grant No. 12274147, 12174123, and 12374347), the Natural Science Foundation of Guangdong Province (Grant No. 2023A1515012368 and 2022A0505030012), and the Natural Science Foundation of Guangzhou (Grant No. 2025A04J2029).

Notes

The authors declare no competing financial interest.

REFERENCES

(1) Zhang, J. L.; Zhong, J. Q.; Lin, J. D.; Hu, W. P.; Wu, K.; Xu, G. Q.; Wee, A. T. S.; Chen, W. Towards Single Molecule Switches. *Chem. Soc. Rev.* **2015**, *44* (10), 2998−3022.

(2) Xu, X.; Gao, C.; Emusani, R.; Jia, C.; Xiang, D. Toward Practical Single-Molecule/Atom Switches. *Adv. Sci.* **2024**, *11* (29), No. 2400877.

(3) Lee, J.; Wu, Y.; Sinev, I.; Masharin, M.; Papadopoulos, S.; Dias, E. J. C.; Wang, L.; Tseng, M. L.; Moon, S.; Yeo, J. S.; Novotny, L.; de Abajo, F. J. G.; Altug, H. Plasmonic Biosensor Enabled by Resonant Quantum Tunnelling. *Nat. Photonics* **2025**, *19* (9), 938−945.

(4) Tang, J.; Guo, Q.; Wu, Y.; Ge, J.; Zhang, S.; Xu, H. Light-Emitting Plasmonic Tunneling Junctions: Current Status and Perspectives. *ACS Nano* **2024**, *18* (4), 2541−2551.

(5) Böckmann, H.; Liu, S.; Müller, M.; Hammud, A.; Wolf, M.; Kumagai, T. Near-Field Manipulation in a Scanning Tunneling Microscope Junction with Plasmonic Fabry-Pérot Tips. *Nano Lett.* **2019**, *19* (6), 3597−3602.

(6) Liu, S.; Wolf, M.; Kumagai, T. Plasmon-Assisted Resonant Electron Tunneling in a Scanning Tunneling Microscope Junction. *Phys. Rev. Lett.* **2018**, *121* (22), No. 226802.

(7) Deeb, C.; Toudert, J.; Pelouard, J. L. Electrically Driven Nanogap Antennas and Quantum Tunneling Regime. *Nanophotonics* **2023**, *12* (15), 3029−3051.

(8) Ludwig, M.; Aguirregabiria, G.; Ritzkowsky, F.; Rybka, T.; Marinica, D. C.; Aizpurua, J.; Borisov, A. G.; Leitenstorfer, A.; Brida, D. Sub-Femtosecond Electron Transport in a Nanoscale Gap. *Nat. Phys.* **2020**, *16* (3), 341−345.

(9) Rybka, T.; Ludwig, M.; Schmalz, M. F.; Knittel, V.; Brida, D.; Leitenstorfer, A. Sub-Cycle Optical Phase Control of Nanotunnelling in the Single-Electron Regime. *Nat. Photonics* **2016**, *10* (10), 667−670.

(10) Borisov, A. G.; Ma, B.; Zapata-Herrera, M.; Babaze, A.; Krüger, M.; Aizpurua, J. Femtosecond Optical-Field-Driven Currents in Few-Nanometer-Size Gaps with Hot Electron Injection into Metallic Leads. *ACS Photonics* **2025**, *12* (4), 2137−2150.

(11) Tang, Y.; Prakash, S.; Nandi, P.; Ariando, A.; Agrawal, A.; Harutyunyan, H. Light-Matter Interaction in Ultrastable Tunneling Nanogaps. *ACS Nano* **2025**, *19* (30), 27204−27214.

(12) Ludwig, M.; Kazansky, A. K.; Aguirregabiria, G.; Marinica, D. C.; Falk, M.; Leitenstorfer, A.; Brida, D.; Aizpurua, J.; Borisov, A. G. Active Control of Ultrafast Electron Dynamics in Plasmonic Gaps Using an Applied Bias. *Phys. Rev. B* **2020**, *101* (24), No. 241412.

(13) Guo, G.-C.; Png, C. E.; Gong, Q.; Xu, D.; Xiao, Y.-F.; Xiong, X.; Ren, X.-F.; Wu, L. Quantum Plasmonics: New Opportunity in Fundamental and Applied Photonics. *Adv. Opt. Photonics* **2018**, *10* (4), 703−756.

(14) Ding, T.; Tserkezis, C.; Mystilidis, C.; Vandenbosch, G. A. E.; Zheng, X. Quantum Mechanics in Plasmonic Nanocavities: From Theory to Applications. *Adv. Phys. Res.* **2025**, *4* (4), No. 2400144.

(15) Zhu, W.; Esteban, R.; Borisov, A. G.; Baumberg, J. J.; Nordlander, P.; Lezec, H. J.; Aizpurua, J.; Crozier, K. B. Quantum Mechanical Effects in Plasmonic Structures with Subnanometre Gaps. *Nat. Commun.* **2016**, *7* (1), No. 11495.

(16) Savage, K. J.; Hawkeye, M. M.; Esteban, R.; Borisov, A. G.; Aizpurua, J.; Baumberg, J. J. Revealing the Quantum Regime in Tunnelling Plasmonics. *Nature* **2012**, *491* (7425), 574−577.

(17) Tame, M. S.; McEnery, K. R.; Özdemir, Ş. K.; Lee, J.; Maier, S. A.; Kim, M. S. Quantum Plasmonics. *Nat. Phys.* **2013**, *9* (6), 329−340.

(18) Jose, J.; Schumacher, L.; Jalali, M.; Haberfehlner, G.; Svejda, J. T.; Erni, D.; Schlücker, S. Particle Size-Dependent Onset of the Tunneling Regime in Ideal Dimers of Gold Nanospheres. *ACS Nano* **2022**, *16* (12), 21377−21387.

(19) Cha, H.; Yoon, J. H.; Yoon, S. Probing Quantum Plasmon Coupling Using Gold Nanoparticle Dimers with Tunable Interparticle Distances down to the Subnanometer Range. *ACS Nano* **2014**, *8* (8), 8554−8563.

(20) Jung, H.; Cha, H.; Lee, D.; Yoon, S. Bridging the Nanogap with Light: Continuous Tuning of Plasmon Coupling between Gold Nanoparticles. *ACS Nano* **2015**, *9* (12), 12292−12300.

(21) Marinica, D. C.; Kazansky, A. K.; Nordlander, P.; Aizpurua, J.; Borisov, A. G. Quantum Plasmonics: Nonlinear Effects in the Field Enhancement of a Plasmonic Nanoparticle Dimer. *Nano Lett.* **2012**, *12* (3), 1333−1339.

(22) Scholl, J. A.; García-Etxarri, A.; Koh, A. L.; Dionne, J. A. Observation of Quantum Tunneling between Two Plasmonic Nanoparticles. *Nano Lett.* **2013**, *13* (2), 564−569.

(23) Teperik, T. V.; Nordlander, P.; Aizpurua, J.; Borisov, A. G. Robust Subnanometric Plasmon Ruler by Rescaling of the Nonlocal Optical Response. *Phys. Rev. Lett.* **2013**, *110* (26), No. 263901.

(24) Zuloaga, J.; Prodan, E.; Nordlander, P. Quantum Description of the Plasmon Resonances of a Nanoparticle Dimer. *Nano Lett.* **2009**, *9* (2), 887−891.

(25) Song, P.; Nordlander, P.; Gao, S. Quantum Mechanical Study of the Coupling of Plasmon Excitations to Atomic-Scale Electron Transport. *J. Chem. Phys.* **2011**, *134* (7), No. 074701.

(26) Lee, K. J.; Kim, S.; Hong, W.; Park, H.; Jang, M. S.; Yu, K.; Choi, S. Y. Observation of Wavelength-Dependent Quantum Plasmon

Tunneling with Varying the Thickness of Graphene Spacer. *Sci. Rep.* **2019**, *9* (1), No. 1199.
(27) Yang, L.; Wang, H.; Fang, Y.; Li, Z. Polarization State of Light Scattered from Quantum Plasmonic Dimer Antennas. *ACS Nano* **2016**, *10* (1), 1580−1588.
(28) Jalali, M.; Jalali, M.; Jose, J.; Schlücker, S.; Erni, D. Curvature Dependent Onset of Quantum Tunneling in Subnanometer Gaps. *Opt. Express* **2023**, *31* (21), 35387−35395.
(29) Wu, Y.; Konečná, A.; Cho, S. H.; Milliron, D. J.; Hachtel, J. A.; García de Abajo, F. J. Singular and Nonsingular Transitions in the Infrared Plasmons of Nearly Touching Nanocube Dimers. *ACS Nano* **2024**, *18* (23), 15130−15138.
(30) Knebl, D.; Hörl, A.; Trügler, A.; Kern, J.; Krenn, J. R.; Puschnig, P.; Hohenester, U. Gap Plasmonics of Silver Nanocube Dimers. *Phys. Rev. B* **2016**, *93* (8), No. 081405.
(31) Tan, S. F.; Wu, L.; Yang, J. K. W.; Bai, P.; Bosman, M.; Nijhuis, C. A. Quantum Plasmon Resonances Controlled by Molecular Tunnel Junctions. *Science* **2014**, *343* (6178), 1496−1499.
(32) Pérez-González, O.; Zabala, N.; Borisov, A. G.; Halas, N. J.; Nordlander, P.; Aizpurua, J. Optical Spectroscopy of Conductive Junctions in Plasmonic Cavities. *Nano Lett.* **2010**, *10* (8), 3090−3095.
(33) Barrio, J.; Manzorro, R.; Sánchez-Iglesias, A.; Rodríguez-San-Miguel, D.; Coronado-Puchau, M.; Moreno, C.; Langer, J.; Fernández-Domínguez, A. I.; Trasobares, S.; Liz-Marzán, L. M.; Zamora, F.; Juárez, B. H. Influence of the Gap Distance and Morphology on the Plasmon Modes of Gold Nanocube Dimers. *Adv. Opt. Mater.* **2025**, *13* (15), No. 2500042.
(34) Grillet, N.; Manchon, D.; Bertorelle, F.; Bonnet, C.; Broyer, M.; Cottancin, E.; Lermé, J.; Hillenkamp, M.; Pellarin, M. Plasmon Coupling in Silver Nanocube Dimers: Resonance Splitting Induced by Edge Rounding. *ACS Nano* **2011**, *5* (12), 9450−9462.
(35) Zhang, S.; Xu, H. Tunable Dark Plasmons in a Metallic Nanocube Dimer: Toward Ultimate Sensitivity Nanoplasmonic Sensors. *Nanoscale* **2016**, *8* (28), 13722−13729.
(36) Lu, Z.; Ji, J.; Ye, H.; Zhang, H.; Zhang, S.; Xu, H. Quantifying the Ultimate Limit of Plasmonic Near-Field Enhancement. *Nat. Commun.* **2024**, *15* (1), No. 8803.
(37) Chikkaraddy, R.; Zheng, X.; Benz, F.; Brooks, L. J.; De Nijs, B.; Carnegie, C.; Kleemann, M. E.; Mertens, J.; Bowman, R. W.; Vandenbosch, G. A. E.; Moshchalkov, V. V.; Baumberg, J. J. How Ultranarrow Gap Symmetries Control Plasmonic Nanocavity Modes: From Cubes to Spheres in the Nanoparticle-on-Mirror. *ACS Photonics* **2017**, *4* (3), 469−475.
(38) Akselrod, G. M.; Argyropoulos, C.; Hoang, T. B.; Ciracì, C.; Fang, C.; Huang, J.; Smith, D. R.; Mikkelsen, M. H. Probing the Mechanisms of Large Purcell Enhancement in Plasmonic Nanoantennas. *Nat. Photonics* **2014**, *8* (11), 835−840.
(39) Esteban, R.; Borisov, A. G.; Nordlander, P.; Aizpurua, J. Bridging Quantum and Classical Plasmonics with a Quantum-Corrected Model. *Nat. Commun.* **2012**, *3* (1), No. 825.
(40) Esteban, R.; Zugarramurdi, A.; Zhang, P.; Nordlander, P.; García-Vidal, F. J.; Borisov, A. G.; Aizpurua, J. A Classical Treatment of Optical Tunneling in Plasmonic Gaps: Extending the Quantum Corrected Model to Practical Situations. *Faraday Discuss.* **2015**, *178*, 151−183.
(41) Aguirregabiria, G. Theoretical Study of the Linear and Nonlinear Optical Response of Plasmonic Tunneling Gaps, Ph.D. Dissertation; University of the Basque Country: Bilbao, 2018, http://hdl.handle.net/10261/180267.
(42) Li, G. C.; Lei, D.; Qiu, M.; Jin, W.; Lan, S.; Zayats, A. V. Light-Induced Symmetry Breaking for Enhancing Second-Harmonic Generation from an Ultrathin Plasmonic Nanocavity. *Nat. Commun.* **2021**, *12* (1), No. 4326.
(43) Kim, J. Y.; Han, M. G.; Lien, M. B.; Magonov, S.; Zhu, Y.; George, H.; Norris, T. B.; Kotov, N. A. Dipole-like Electrostatic Asymmetry of Gold Nanorods. *Sci. Adv.* **2018**, *4* (2), No. e1700682.
(44) Pedrazo-Tardajos, A.; Claes, N.; Wang, D.; Sánchez-Iglesias, A.; Nandi, P.; Jenkinson, K.; De Meyer, R.; Liz-Marzán, L. M.; Bals, S. Direct Visualization of Ligands on Gold Nanoparticles in a Liquid Environment. *Nat. Chem.* **2024**, *16* (8), 1278−1285.
(45) Liu, D.; Wu, T.; Zhang, Q.; Wang, X.; Guo, X.; Su, Y.; Zhu, Y.; Shao, M.; Chen, H.; Luo, Y.; Lei, D. Probing the In-Plane Near-Field Enhancement Limit in a Plasmonic Particle-on-Film Nanocavity with Surface-Enhanced Raman Spectroscopy of Graphene. *ACS Nano* **2019**, *13* (7), 7644−7654.
(46) Bochterle, J.; Neubrech, F.; Nagao, T.; Pucci, A. Angstrom-Scale Distance Dependence of Antenna-Enhanced Vibrational Signals. *ACS Nano* **2012**, *6* (12), 10917−10923.
(47) Rivest, J. B.; Li, G.; Sharp, I. D.; Neaton, J. B.; Milliron, D. J. Phosphonic Acid Adsorbates Tune the Surface Potential of TiO2 in Gas and Liquid Environments. *J. Phys. Chem. Lett.* **2014**, *5* (14), 2450−2454.
(48) Hajisalem, G.; Nezami, M. S.; Gordon, R. Probing the Quantum Tunneling Limit of Plasmonic Enhancement by Third Harmonic Generation. *Nano Lett.* **2014**, *14* (11), 6651−6654.
(49) Zhang, Q.; Li, G. C.; Lo, T. W.; Lei, D. Y. Polarization-Resolved Optical Response of Plasmonic Particle-on-Film Nanocavities. *J. Opt.* **2018**, *20* (2), No. 024010.
(50) Li, G. C.; Zhang, Y. L.; Lei, D. Y. Hybrid Plasmonic Gap Modes in Metal Film-Coupled Dimers and Their Physical Origins Revealed by Polarization Resolved Dark Field Spectroscopy. *Nanoscale* **2016**, *8* (13), 7119−7126.
(51) Tserkezis, C.; Esteban, R.; Sigle, D. O.; Mertens, J.; Herrmann, L. O.; Baumberg, J. J.; Aizpurua, J. Hybridization of Plasmonic Antenna and Cavity Modes: Extreme Optics of Nanoparticle-on-Mirror Nanogaps. *Phys. Rev. A* **2015**, *92* (5), No. 053811.
(52) Aghdaee, M. R.; Goodwin, M. J.; Ojambati, O. S. Optical Detection of Single Sub-15 Nm Objects Using Elastic Scattering Strong Coupling. *Nat. Commun.* **2025**, *16* (1), No. 8101.
(53) Benz, F.; Tserkezis, C.; Herrmann, L. O.; De Nijs, B.; Sanders, A.; Sigle, D. O.; Pukenas, L.; Evans, S. D.; Aizpurua, J.; Baumberg, J. J. Nanooptics of Molecular-Shunted Plasmonic Nanojunctions. *Nano Lett.* **2015**, *15* (1), 669−674.
(54) Cui, X.; Qin, F.; Lai, Y.; Wang, H.; Shao, L.; Chen, H.; Wang, J.; Lin, H. Q. Molecular Tunnel Junction-Controlled High-Order Charge Transfer Plasmon and Fano Resonances. *ACS Nano* **2018**, *12* (12), 12541−12550.
(55) Wu, Y.; Konečná, A.; Cho, S. H.; Milliron, D. J.; Hachtel, J. A.; García de Abajo, F. J. Singular and nonsingular Transitions in the Infrared Plasmons of Nearly Touching Nanocube Dimers. *ACS Nano* **2024**, *18* (23), 15130−15138.
(56) Guo, G.-C.; Png, C. E.; Gong, Q.; Xu, D.; Xiao, Y.-F.; Xiong, X.; Ren, X.-F.; Wu, L. Quantum plasmonics: New Opportunity in Fundamental and Applied Photonics. *Adv. Opt. Photonics* **2018**, *10* (4), 703−756.
(57) Zhou, Z. K.; Liu, J.; Bao, Y.; Wu, L.; Png, C. E.; Wang, X. H.; Qiu, C. W. Quantum Plasmonics Get Applied. *Prog. Quantum Electron.* **2019**, *65*, 1−20.
(58) Love, J. C.; Estroff, L. A.; Kriebel, J. K.; Nuzzo, R. G.; Whitesides, G. M. Self-Assembled Monolayers of Thiolates on Metals as a Form of Nanotechnology. *Chem. Rev.* **2005**, *105* (4), 1103−1169.

https://doi.org/10.1021/acsphotonics.5c02595
ACS Photonics 2026, 13, 1810−1817